A Dual-Band Frequency Selective Surface with Angular Stability

Kai-Da Xu [1, 2, *] Shangjing Xi[1] and Qiang Chen[2]
[1]School of Information and Communications Engineering, Xi'an Jiaotong University, Xi'an 710049, China
[2]Department of Communications Engineering, Tohoku University, Sendai, Japan
*Email: kaidaxu@ieee.org

***Abstract*— In this paper, a three-metal-layer-based compact dual-band frequency selective surface (FSS) is presented with enhanced angular stability and low insertion loss (IL). For the dual-band FSS structure design, the metal square ring in the middle layer facilitates coupling between the top and bottom metal structures. The designed FSS can generate four transmission zeros (TZs) positioned on both sides of each passband. The operating frequencies of the dual-band FSS are at 5.13 and 10.06 GHz, whose fractional bandwidths are 24.2% and 10.9%, respectively. The proposed dual-band FSS maintains insensitive performance on the incident polarization and angle.**

***Keywords*—Dual-band; equivalent circuit model; frequency selective surface; transmission zero.**

I. Introduction

Frequency selective surfaces (FSSs) are two-dimensional (2D) periodic structures for selectively transmitting or blocking electromagnetic waves at specific frequencies [1-10], where periodic metallized patterns are typically etched above the dielectric substrates. Thanks to their filtering capabilities, FSSs are valuable in numerous applications, such as rasorbers and radomes [2][5].

Particularly in modern communication systems, FSSs with independently controllable multiple operating bands are highly needed. Additionally, there is a demand for thin FSSs that exhibit high-selectivity passband or stopband [6][8]. During the design and optimization process, using an equivalent circuit model (ECM) is usually employed, which can offer benefits in analyzing and adjusting parameters of the FSSs effectively [9][10].

In this paper, a new dual-band FSS is designed based on multilayer metal cascaded structure. The designed FSS achieves four transmission zeros (TZs) at the edges of its two passbands. It utilizes the mutual coupling among its three metallic layers, significantly enhancing its frequency selectivity. Moreover, it offers several key benefits, including efficient stopband suppression, insensitivity to polarization of incident wave, and stable performance under various incident angles. The unit cell size is roughly 0.137λ*0.137λ.

II. Analysis of the Proposed Dual-Band FSS

Fig. 1(a) illustrates the unit cell configuration of the dual-band FSS, which consists of three metallic layers divided by two identical substrate layers. The FSS unit cell of the top or bottom layer consists of a square ring and four meandering thin strip lines with four triangular patches at the end, as demonstrated in Fig. 1(b). Besides, Fig. 1(c) shows the middle layer of the FSS unit cell, which is a metallic square ring. The FSS is constructed on an F4B-2 substrate characterized by a relative dielectric constant of 2.65 and a thickness (h) of 2 mm.

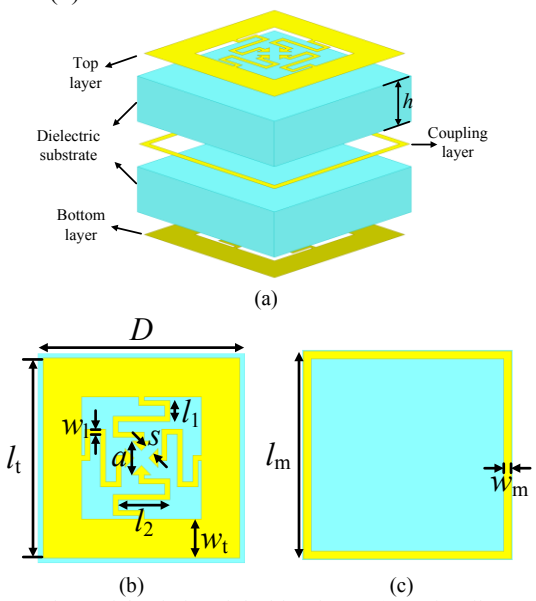

Fig. 1. Topology of the designed dual-band FSS. (a) Unit cell structure of the presented FSS. (b) The top/bottom layer of FSS unit cell. (c) The middle layer of FSS unit cell.

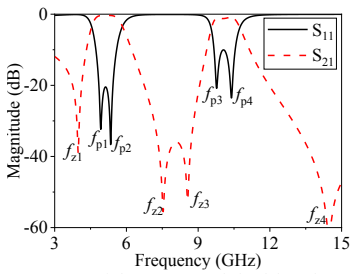

Fig. 2. Frequency response of the presented dual-band FSS.

Fig. 2 displays the simulation performance of the dual-band FSS structure, with corresponding dimensions specified in Table I. It distinctly shows four TZs (f_{z1}, f_{z2}, f_{z3}, and f_{z4}) positioned on each side of the two passbands, significantly enhancing the high frequency selectivity of the presented dual-band FSS. Additionally, the designed dual-band FSS has two transmission poles (TPs) in each passband. The maximum simulated insertion losses (ILs) in the two passbands are 0.38 dB and 1.22 dB, and the corresponding 3-dB bandwidths are 24.2% and 10.9%, respectively.

To illustrate the generation mechanism of TZs, an ECM is proposed, as depicted in Fig. 3. This model treats the gap between unit cells on the top or bottom layer as a capacitor C_1. The loop can be equivalent to an inductor L_1. Similarly, the gaps among triangular patches and the meandering lines

979-8-3503-8331-7/24/$31.00 @2024 IEEE

2024 IEEE International Conference on Computational Electromagnetics (ICCEM) | 979-8-3503-8331-7/24/$31.00 ©2024 IEEE | DOI: 10.1109/ICCEM60619.2024.10558961

are represented by capacitor C_2 and inductor L_2, respectively. The gaps between unit cells are modeled on the middle layer with a capacitor C_3, and the square ring corresponds to an inductor L_3. The structure of the circuit, comprising the serial connections of L_1–C_1, L_2–C_2, and L_3–C_3, introduces TZs into the filtering response. The mutual inductive coupling is represented by coefficients K_1 and K_2 for the coupling effect between two inductors L_1 and two inductors L_2, respectively. In addition, K_3 represents the mutual inductive coupling effect between inductors L_1 and L_3. Notably, reducing the substrate's thickness can enhance this coupling effect. The ECM component values are tabulated in Table II. Adjusting these parameters enables the realization of four TZs near the skirts of the two passbands. The validity of this design is confirmed through both full-wave and circuit simulation results, as illustrated in Fig. 4.

TABLE I
GEOMETRIC PARAMETERS OF THE PRESENTED DUAL-BAND FSS

Parameter	D	l_t	l_1	l_2	w_t
Value (mm)	8.0	7.6	0.8	2.0	1.48
Parameter	w_1	a	s	l_m	w_m
Value (mm)	0.2	1.3	0.4	7.9	0.3

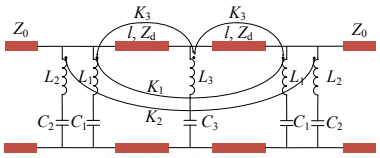

Fig. 3. ECM of the designed dual-band FSS.

TABLE II
VALUES OF THE EQUIVALENT CIRCUIT COMPONENTS

C_1 (fF)	C_2 (fF)	C_3 (fF)	L_1 (nH)	L_2 (nH)	L_3 (nH)
69	72	308	5.45	1.69	5.53
K_1	K_1	K_3	Z_0 (Ω)	l (°)	Z_d (Ω)
0.003	0.001	0.09	377	24	231.6

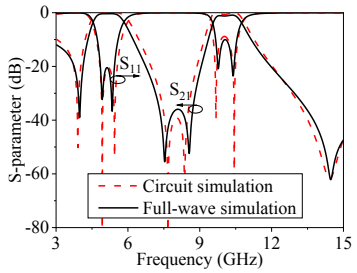

Fig. 4. Analysis of S-parameters: full-wave simulation versus ECM simulation.

Fig. 5 displays the simulated results of the presented dual-band FSS under varying angles and polarizations of incident wave. This dual-band FSS exhibits excellent angle stability, consistently performing from 0° to 40° across different polarizations. As the incidence angle is altered from 0° to 40°, there is a minor shift in the center frequency of the low-frequency passband for transverse electric (TE) polarization. Conversely, the center frequency position of the high-frequency passband remains unchanged, showing no shift even as the incidence angle extends to 40°. For transverse magnetic (TM) polarization, an increase in the incident angle causes a slight upward shift in the center frequencies of both passbands.

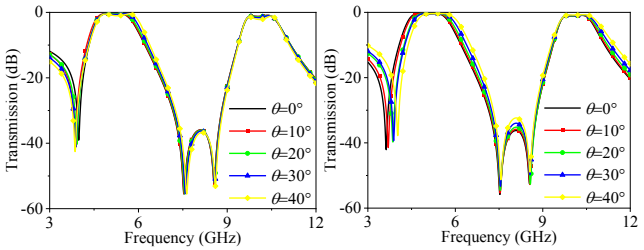

Fig. 5. The simulated outcomes for the designed dual-band FSS at different incident angles are shown for (a) TE polarization, and (b) TM polarization.

III. CONCLUSION

This paper introduces a dual-band FSS characterized by low IL and excellent angular stability. Four TZs at each side of the passbands significantly enhance frequency selectivity. The proposed FSS has some advantages, such as compact structure, stability under oblique incidence, and insensitivity to polarization of incident wave. These features make it a promising solution for various emerging communication systems.

REFERENCES

[1] B. A. Munk, Frequency Selective Surfaces: Theory and Design. New York, NY, USA: Wiley, 2000.

[2] T. K. Wu, Frequency Selective Surface and Grid Array. New York, NY, USA: Wiley, 1995.

[3] R. Mittra, C. H. Chan, and T. Cwik, "Techniques for analyzing frequency selective surfaces—A review," *Proc. IEEE*, vol. 76, no. 12, pp. 1593–1615, Dec. 1989.

[4] Y. Shi and X. Y. Liu, "Dual-Polarized Frequency Selective Rasorber with Two Wide Transmission Bands," *IEEE Trans. Antennas Propag.*, vol. 71, no. 7, pp. 6260-6265, July 2023.

[5] K. Duan, K. Chen, T. Jiang, J. Zhao and Y. Feng, "Ultrawideband Frequency Selective Radome Utilizing 2.5-D Lossy Layers," *IEEE Antennas Wireless Propag. Lett.*, vol. 22, no. 10, pp. 2427-2431, Oct. 2023,

[6] G. Xu, G. V. Eleftheriades and S. V. Hum, "Generalized Synthesis Technique for High-Order Low-Profile Dual-Band Frequency Selective Surfaces," *IEEE Trans. Antennas Propag.*, vol. 66, no. 11, pp. 6033-6042, Nov. 2018.

[7] M. A. Al-Joumayly and N. Behdad, "A generalized method for synthesizing low-profile, band-pass frequency selective surfaces with nonresonant constituting elements," *IEEE Trans. Antennas Propag.*, vol. 58, no. 12, pp. 4033–4041, Dec. 2010.

[8] N. Behdad and M. A. Al-Joumayly, "A generalized synthesis procedure for low-profile, frequency selective surfaces with odd-order bandpass responses," *IEEE Trans. Antennas Propag.*, vol. 58, no. 7, pp. 2460–2464, Jul. 2010.

[9] M. Hussein, J. Zhou, Y. Huang and B. Al-Juboori, "A Low-Profile Miniaturized Second-Order Bandpass Frequency Selective Surface," *IEEE Antennas Wireless Propag. Lett.*, vol. 16, pp. 2791-2794, 2017.

[10] S. Xi, K-D. Xu, S. Yang, X. Ren and W. Wu, "X-band frequency selective surface with low loss and angular stability," *AEU-Int J Electron C.*, vol. 173, p. 154990, Jan. 2024.